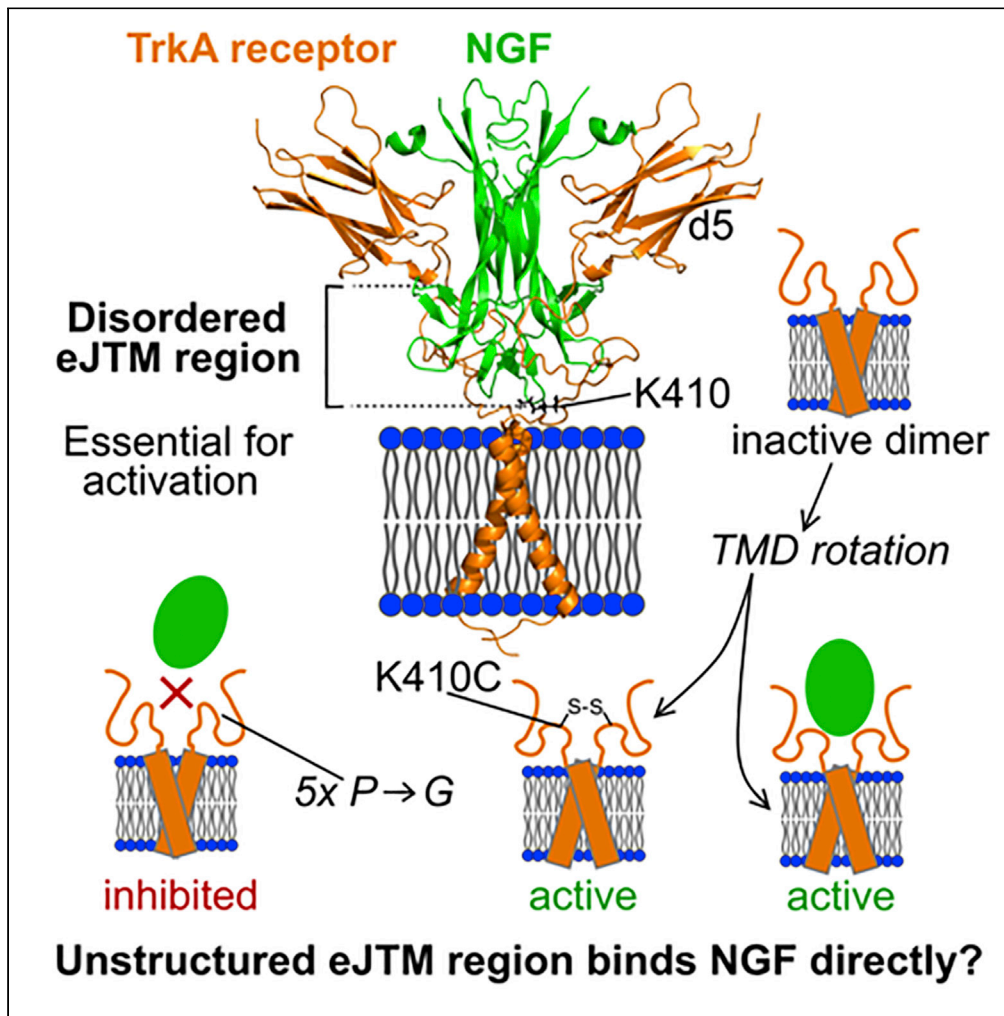**Article**

Intrinsically disordered regions couple the ligand binding and kinase activation of Trk neurotrophin receptors

Erik F. Kot, María
L. Franco,
Ekaterina V.
Vasilieva, ...,
Sergey A.
Goncharuk,
Konstantin S.
Mineev, Marçal
Vilar

aars@nmr.ru (A.S.A.)
ms.goncharuk@gmail.com
(S.A.G.)
konstantin.mineev@gmail.com
(K.S.M.)
mvilar@ibv.csic.es (M.V.)

Highlights

Extracellular
juxtamembrane region is
required for NGF binding
and TrkA activation

TrkA extracellular
juxtamembrane region is
unstructured and flexible

This region couples
neurotrophin-binding and
transmembrane domain
rotation

The extracellular
juxtamembrane region
might play a role in
neurotrophin recognition

Article

Intrinsically disordered regions couple the ligand binding and kinase activation of Trk neurotrophin receptors

Erik F. Kot,[2,4] María L. Franco,[3,4] Ekaterina V. Vasilieva,[1] Alexandra V. Shabalkina,[1,2] Alexander S. Arseniev,[1,2,*] Sergey A. Goncharuk,[1,2,*] Konstantin S. Mineev,[1,2,*] and Marçal Vilar[3,5,*]

SUMMARY

Receptor tyrosine kinases (RTKs) are key players in development and several diseases. Understanding the molecular mechanism of RTK activation by its ligand could lead to the design of new RTK inhibitors. How the extracellular domain is coupled to the intracellular kinase domain is a matter of debate. Ligand-induced dimerization and ligand-induced conformational change of pre-formed dimers are two of the most proposed models. Recently we proposed that TrkA, the RTK for nerve growth factor (NGF), is activated by rotation of the transmembrane domain (TMD) pre-formed dimers upon NGF binding. However, one of the unsolved issues is how the ligand binding is conformationally coupled to the TMD rotation if unstructured extracellular juxtamembrane (eJTM) regions separate them. Here we use nuclear magnetic resonance in bicelles and functional studies to demonstrate that eJTM regions from the Trk family are intrinsically disordered and couple the ligand-binding domains and TMDs possibly via the interaction with NGF.

INTRODUCTION

The molecular mechanisms of activation of Trks have been poorly studied when compared with those of other receptor tyrosine kinase (RTK) family members (Endres et al., 2014; Lemmon and Schlessinger, 2010). The first three extracellular domains of Trks consist of a leucine-rich region, LRR (Trk-d1), flanked by two cysteine-rich domains (Trk-d2 and Trk-d3) (Figure 1A). The fourth and fifth domains (Trk-d4 and Trk-d5) are immunoglobulin (Ig)-like domains, and these are followed by a 30-residue-long linker that connects the extracellular portion of the receptor to the single transmembrane domain and a juxtamembrane intracellular region that is connected to the kinase domain. The nerve growth factor (NGF)-binding domain is located in the Trk-d5 domain (Ultsch et al., 1999; Wehrman et al., 2007; Wiesmann et al., 1999), although other domains of extracellular TrkA also participate. Analysis of TrkA constructs by swapping the extracellular domains between TrkA and TrkB receptors (Zaccaro et al., 2001), or the identification of a constitutively active point mutation in the d4 domain of TrkA extracellular domain (Arevalo et al., 2001), suggested that regions far from the NGF-binding domain (TrkA-d5) also play a role in NGF binding and/or TrkA activation by NGF.

One of the unsolved issues in the activation mechanism of RTKs is how the ligand binding is conformationally coupled to the dimerization of the TMD if flexible juxtamembrane regions separate them. Recently it has been shown that TrkA activation occurs through a rotation of the TMD induced by NGF binding (Franco et al., 2020) and that it is modulated by the interaction with low-affinity neurotrophin receptor p75 (Franco et al., 2021). In the case of TrkA the extracellular juxtamembrane (eJTM) domain consists of a 30-residue-long region rich in proline residues (green in Figure 1A). The role of eJTM in TrkA activation by NGF is not clear. The biochemical data suggest an important role of some charged residues of the eJTM in the binding to NGF (Urfer et al., 1998). However, the structural data of this region are absent in the two crystal structures of TrkA with NGF reported (Wehrman et al., 2007; Wiesmann et al., 1999) suggesting a high flexibility of the region. One caveat of the crystallographic studies is that they were done in solution with a truncated C terminus in the absence of TMD, a condition quite different from the restricted conformational movement expected when the eJTM is connected to the TMD attached to the plasma membrane.

Figure 1. TrkA domains and functional assays of TrkA-ΔeJTM

(A) A drawing showing the location of the protein domains is shown on the left of an intrinsic order prediction using IUPred2A (https://iupred2a.elte.hu/) plotted versus the residue number of TrkA. A value above 0.5 indicates disorder. The eJTM region corresponding to residues 383–414 is shown in green. The residues previously shown to have an effect of NGF binding to TrkA when mutated are shown in red bold. The proline residues present in this region are shown in black bold. Residues Lys 410 and 411 are shown in blue bold.

(B) Crystal structure of TrkA-d5 domain in complex with NGF (PDB:1www) indicating the residue P349, which is the last residue of TrKA construct observed in the X-ray structure.

(C) Binding assays of biotinylated NGF to TrkA and TrkA-ΔeJTM expressed in HEK293 cells and fitted to one-site binding.

(D) Quantification using TrkA phospho-specific antibodies of cell lysate extracts from HEK293 cells transfected with the indicated constructs and stimulated with NGF for the indicated times (0, 5, and 15 min).

(E) Percentage of differentiated PC12nnr5 cells with NGF transfected with the indicated constructs stimulated with NGF for 48 h. Data are represented as mean ± SEM Error bars represent the SEM of at least three independent experiments. Statistical significance obtained by two-way ANOVA analysis with Bonferroni correction.

Exact p values are shown.

In the present work we investigate the role of TrkA-eJTM region in receptor activation using functional and structural studies with the incorporation of the construct, containing the entire eJTM and TMD regions (D380-K447 of human TrkA), into bicelles and analyzed by nuclear magnetic resonance (NMR). We show that the eJTM region of TrkA plays a key role in mediating the conformational coupling between ligand binding and TrkA activation.

RESULTS

The extracellular juxtamembrane domain is required for NGF binding by TrkA

The eJTM region of TrkA, which is located between the NGF-binding domain (TrkA-d5) and the TMD, is a highly conserved region comprising around 30 residues (Figure 1A, green). *In silico* using the prediction software IUPred2A (Erdős and Dosztányi, 2020; Mészáros et al., 2018) the eJTM is predicted to be disordered (Figure 1A). Interestingly, earlier studies revealed that mutations of some of the residues in the

N-terminal part of the eJTM (E384A/N386A, E388A/D389A, and I391A, human TrkA numbering, red in the Figure 1A) reduced significantly the binding to NGF (Urfer et al., 1998), suggesting a direct contact with the neurotrophin in this region; however, the structural data of this region are absent in the two crystal structures of TrkA with NGF reported (Wehrman et al., 2007; Wiesmann et al., 1999).

To gain an understanding of the role of this region we looked into the reported crystal structures (Figure 1B). There are two X-ray studies of TrkA/NGF complex; the first one reported the structure of the isolated TrkA-d5 with NGF (Wiesmann et al., 1999), and the most recent reported the structure of the full extracellular domain of TrkA with NGF (Wehrman et al., 2007). In the two structures the last residue visible in the crystal is P382 (Figure 1B) and NGF extends further than the C terminus of TrkA protein construct by approximately 20 Å, well beyond the folded TrkA-d5 domain. Based on these structures, deletion of the entire eJTM in the context of a full-length receptor may impair the binding of NGF to TrkA. To show it graphically we modeled the fusion between the TrkA-d5 domain and the TMD (i.e., TrkA with deleted eJTM). The model reveals that NGF binding to the TrkA-d5 domain will make NGF to dive into the lipid bilayer (Figure S1). To probe experimentally this hypothesis, we made the TrkA-ΔeJTM construct, in which the entire eJTM was deleted and the TrkA-d5 domain was directly bound to the TMD. To study the effect of the deletion, we used three functional assays: binding to NGF, activation of TrkA phosphorylation by NGF, and differentiation of PC12 cells with the TrkA/NGF system. For the binding of NGF to TrkA constructs, we used a flow cytometry assay. In this assay we expressed TrkA in HEK293 cells and quantified the binding of TrkA to NGF by using an NGF attached with biotin (NGF-biotin is functional as it induces TrkA activation and PC12 cells differentiation, Figures S2A and S2B) and a streptavidin-Cy2 fluorophore (see STAR Methods). Cells were incubated with different concentrations of NGF-biotin, and the mean fluorescence of the cells was quantified by flow cytometry (Figure S2) and plotted in the Figure 1C. Data were fitted to a one-site binding curve providing a Kd of 4.40×10^{-9} M. By contrast, cells expressing TrkA-ΔeJTM showed low fluorescence labeling indicative of poor NGF binding (Kd approximately. 7.6×10^{-7} M).

Binding to NGF induces the kinase activation of TrkA. As it is shown in Figure 1D, lysates from the HEK293 cells transfected with TrkA and TrkA-ΔeJTM reveal that only TrkA is autophosphorylated by NGF, indicating that TrkA-ΔeJTM is not activated by NGF supporting the binding assays shown earlier. To finalize the functional assays, PC12nnr5 cells that do not express endogenous levels of TrkA were transfected with TrkA and TrkA-ΔeJTM, and the formation of neurites was quantified at 48 h after NGF stimulation. Figure 1E shows the number of cells differentiated indicating that TrkA-ΔeJTM-transfected PC12nnr5 cells do not promote the neurite extension by NGF. In summary, the functional assays showed that TrkA-ΔeJTM cannot bind to NGF, is not activated by NGF, and does not induce cell differentiation. Immunofluorescence localization of TrkA with an antibody against the HA-tag located at the N terminus of TrkA showed that the receptor trafficked correctly to the plasma membrane (Figure S2), suggesting that it was properly folded.

This result indicates that the stretch of 30 residues is somehow required to accommodate NGF between the ligand-binding domain and the transmembrane region.

eJTM of TrkA is unstructured, mobile, and does not interact with lipid bilayer

To further investigate the properties of the juxtamembrane region, we synthesized a protein construct, containing the full eJTM region and a transmembrane helix of TrkA (D380-K447, TrkA-eJTM-TMD, Figures 2A and 2B) with N-terminal His-tag in the cell-free expression system, labeled it with ^{13}C/^{15}N isotopes, purified it, cleaved the His-tag, and incorporated the TrkA-eJTM-TMD into DMPC/CHAPS (1,2-dimyristoyl-*sn*-glycero-3-phosphocholine / 3-[(3-Cholamidopropyl)dimethylammonio]-1-propanesulfonate hydrate) phospholipid bicelles at various lipid-to-detergent ratios, q, for further NMR investigation. These bicelles were previously shown to provide a patch of lipid bilayer and mostly do not affect the structures of water-soluble domains of membrane proteins (Kot et al., 2018; Mineev et al., 2016). The initial analysis with solution NMR revealed that signals, previously shown to correspond to the TrkA TMD (Mineev et al., 2016), disappear at high q values (in large bicelles) due to the slower Brownian tumbling, whereas other cross-peaks experience only the subtle chemical shift perturbation upon q variation (Figure S3). This implies that the extramembrane residues of TrkA-eJTM-TMD experience fast motions, which are not coupled to the motions of the bicelle, and clearly shows that eJTM of TrkA is flexible in the context of TrkA-eJTM-TMD and does not interact with the lipid bilayer of bicelles, only the transient contacts may take place.
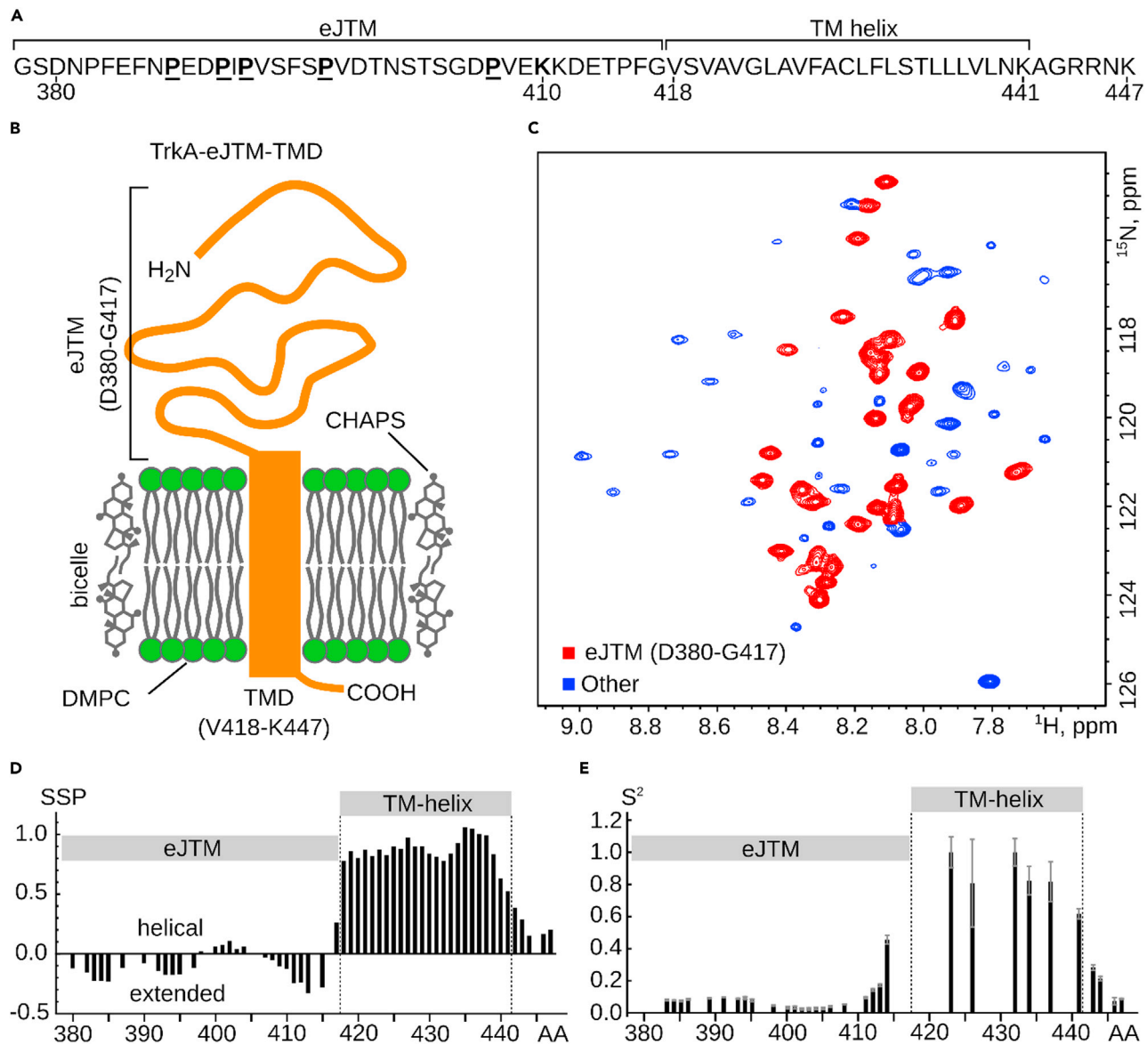
Figure 2. Conformation of TrkA-eJTM

(A) Shown is the TrkA-eJTM-TMD sequence with the boundaries of eJTM and TMD. Five conservative proline residues are highlighted and underlined; K410 is also highlighted.

(B) Schematic drawing showing the TrkA-eJTM-TMD protein incorporated into a DMPC/CHAPS bicelle.

(C) The ^{1}H-^{15}N-Transverse relaxation optimized spectroscopy (TROSY)-HSQC spectrum of wt TrkA-eJTM-TMD. Signals of the JM region (residues D380-G417, eJTM) are colored red.

(D) Secondary structure propensity calculated for the wt TrkA-eJTM-TMD from NMR chemical shifts.

(E) S^2 order parameter measured for the wt TrkA-eJTM-TMD.

The eJTM region is rich in carboxylic groups of Glu and Asp residues, which could in theory coordinate the bivalent cations and stabilize the structure of our construct. To test this possibility we investigated the interaction of TrkA-eJTM-TMD with the most common extracellular divalent cation (Ca^{2+}) and another abundant cation with the distinct coordination properties (Zn^{2+}). Chemical shifts of eJTM did not change upon the addition of specified cations, indicating that the region does not contain any affine metal-binding sites, which could make its structure more regular (Figure S4).

Next we assigned the NMR chemical shifts of the protein and studied its spatial structure using the secondary structure propensity approach (SSP (Marsh et al., 2006), Figures 2D and S5). SSP is a value, calculated based on the protein chemical shifts, which describes the probability of a particular residue to adopt a secondary structure. SSP can vary in the range from −1 to 1, where −1 corresponds to 100% extended conformation and 1 corresponds to the alpha-helix; 0 SSP indicates the random-coil state. According to such an analysis, eJTM of TrkA is mostly unstructured, with some propensity to adopt an extended conformation, but SSP absolute value does not exceed 0.3 (Figure 2D). To assess the mobility of the region we measured the relaxation parameters of ^{15}N nuclei and processed them using the model-free approach (Dosset et al., 2000) assuming the mobility of the protein as a whole equal to the one of the transmembrane helix (Figure S6). Such an analysis provided the order parameters of the eJTM in the range 0–0.1; however, S2 are evidently elevated for the N-terminal part of the region (380–397, Figure 2E).
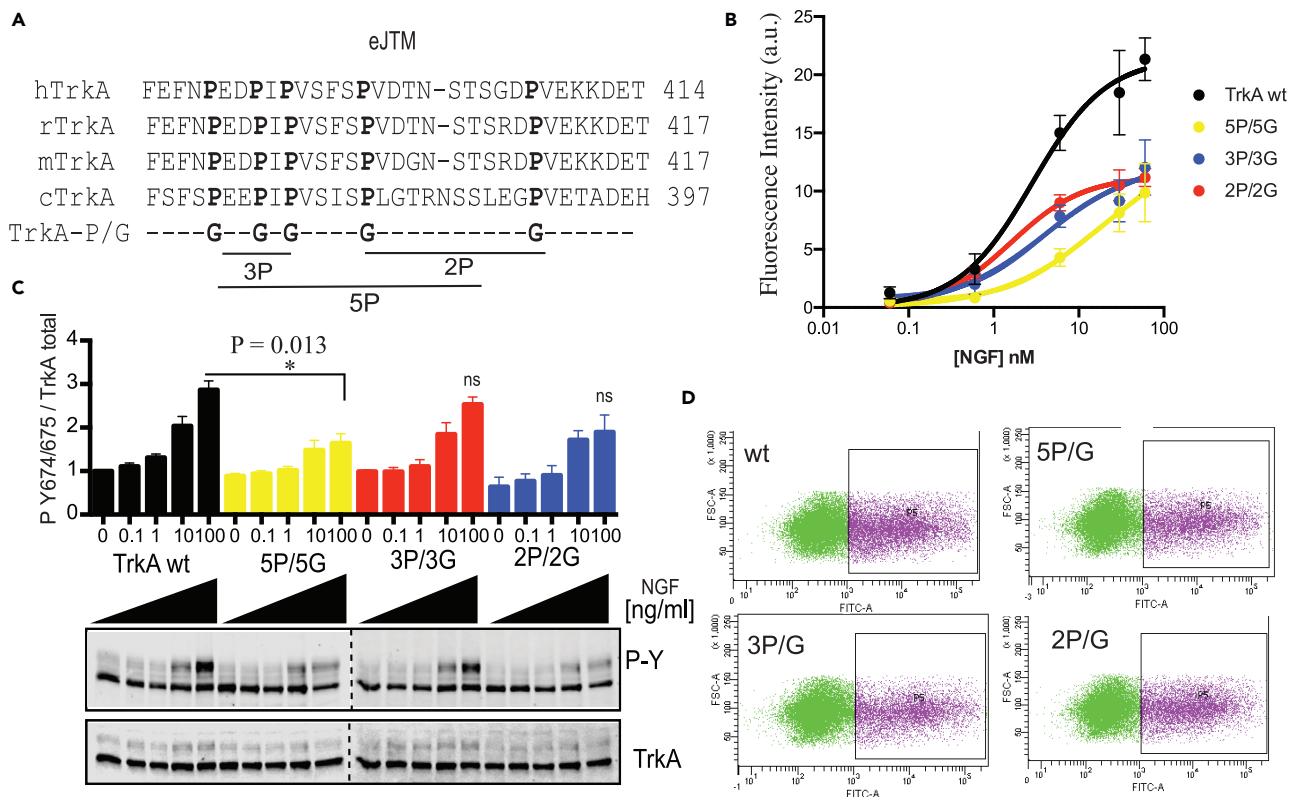
The disordered state of eJTM is supported by the hydrodynamic measurements. We investigated the translational diffusion of bicelle particles in solution, using the designed pseudo-3D^{13}C-edited-double stimulated echo (DSTE) NMR experiment, which allows the simultaneous measurement of diffusion coefficients, corresponding to the lipid and protein signals, with suppression of unwanted contribution of possible convection effect to translational diffusion (Figures 2C and S7). We found out that the bicelles with protein are on average 1.0 nm greater than the "empty" particles. Diffusion of lipid molecules was characterized by the hydrodynamic radius of an equivalent sphere (Rh) equal to 2.8 ± 0.1 nm, which corresponds to the 40-kDa globular protein (Figure S8B) (Tyn and Gusek, 1990). At the same time, the protein diffusion corresponded to Rh of 3.8 ± 0.1 nm, which suggests the apparent mass of the particle equal to 97 kDa. Thus, whereas the real mass of the particle is expected to increase by 7.5 kDa, the increase in the "apparent mass," which characterizes the motions of the particle, is substantially greater. It is well-known that disordered proteins reveal the decelerated diffusion and the increased Rh when compared with the globular ones (Gast and Fiedler, 2012). Therefore, diffusion analysis reveals a highly non-compact state of the disordered eJTM. To summarize this part, the eJTM region of TrkA is disordered, non-compact, and highly mobile, with a slightly restricted mobility in the region 380–397, based on the whole set of NMR data (Figures 2 and S8).

Prolines in eJTM are essential for TrkA activation

According to our data, the information on ligand binding is transduced inside the cell via the extended and unstructured juxtamembrane region. This is possible either due to the direct interaction of eJTM with NGF or due to the restricted mobility of the N-terminal part of the region, which we observe in NMR relaxation data (Figure 2E). In this regard, several conserved and spaced Pro residues in the eJTM (Figure 1A) could play a role in TrkA activation. To test the hypothesis, we substituted all five of the conserved Pro residues to Gly, generating the mutant TrkA-5P/G (Figure 3A). We performed the same functional assays as with the TrkA-ΔeJTM: binding to NGF and activation by NGF. Although the TrkA-5P/G-transfected cells bind to NGF, as opposed to the TrkA-ΔeJTM (Figure 3B), they do it with a lower affinity than the control TrkA-wt-transfected cells. TrkA-5P/G autophosphorylation is less sensitive to the lower concentrations of NGF than TrkA-wt autophosphorylation (Figure 3C). TrkA-5P/G is correctly expressed at the plasma membrane as determined by flow cytometry and immunofluorescence (Figure 3D). Thus, the proline residues in eJTM are necessary for the proper NGF-induced TrkA activation. To further characterize the role of the Pro residues we made two different constructs, where only the three Pro residues located in the most N-terminal region of the eJTM (3P/G) or the two Pro most far from the N terminus (2P/G) were mutated. As shown in the Figure 3, the 2P/G showed an impact on TrkA activation, although not significant statistically, indicating that the region 397–407 could play a role for this function (Figure 3C). However, in terms of NGF binding, the contribution of 2P/G and 3P/G is not significantly different from that of the 5P/G mutant. This suggests that the global change of the eJTM mobility could play a role in TrkA activation by NGF.

Substitution of proline residues does not affect the mobility of the TrkA eJTM

As a next step, we synthesized the TrkA-eJTM-TMD with 5P/G mutations, TrkA-eJTM-TMD-5P/G, and studied the structure and mobility of the eJTM analogously to the wild-type protein (Figures 4A–4C and S9–S11). The mutations left the structure of TMD unaffected according to the NMR spectra, as cross-peaks that correspond to the TMD remained at their positions (Figure 4A). As one can see, the mobility of eJTM also changed insubstantially—the distribution of generalized order parameters along the eJTM is identical in the mutant and wild-type TrkA (Figure 4B). The mutant eJTM-5P/G is still disordered; however, instead of the extended conformation, a slight propensity to form α-helices is observed in the region 387–407 (Figure 4C). This may indicate that in the mutant protein, the eJTM region tends to be more compact, which

A

eJTM

```
hTrkA   FEFNPEDPIPVSFSPVDTN-STSGDPVEKKDET  414
rTrkA   FEFNPEDPIPVSFSPVDTN-STSRDPVEKKDET  417
mTrkA   FEFNPEDPIPVSFSPVDGN-STSRDPVEKKDET  417
cTrkA   FSFSPEEPIPVSISPLGTRNSSLEGPVETADEH  397
TrkA-P/G ----G--G-G----G----------G------
```

3P
2P
5P

B

C

D

Figure 3. Functional assays of TrkA-eJTM-P/G mutants

(A) Protein sequence alignment of the eJTM region of TrkA between different species: human, rat, mouse, and chicken. The position of the Pro residues studied is shown in bold. Below the protein sequence are shown the locations of 2P, 3P, and 5P discussed in the text.

(B) Binding assays of biotinylated NGF to the indicated constructs of TrkA expressed in HEK293 cells and fitted to one-site binding. Paired t test showed significant differences between TrkA-wt and TrkA-5P/5G with a p = 0.036.

(C) Western blot and quantification using TrkA phospho-specific antibodies of cell lysate extracts from HEK293 cells transfected with the indicated constructs and stimulated with increasing concentration of NGF (0, 0.1, 1, 10, and 100 ng/mL) for 15 min. Data are represented as mean ± SEM. Error bars represent the SEM of at least three independent experiments. Statistical significance obtained by ordinary one-way ANOVA analysis with Dunnett's multiple comparison test. Exact p values are shown. ns, not significant.

(D) FITC-labeled HEK293 cells transfected with the indicated TrkA constructs incubated with a FITC-labeled antibody against the N-terminal region of TrkA show that all constructs are equally expressed at the plasma membrane.

leaves less space for the bound ligand and decreases the overall TrkA affinity to NGF (Figure 3). This assumption is in agreement with the hydrodynamic data. We measured the diffusion of protein by NMR using the Heteronuclear Single Quantum Coherence (HSQC)-DSTE experiment (Figure S12A), and Rh of TrkA-eJTM-TMD-5P/G is 0.22 ± 0.07 nm lower than that of the wild-type protein, which implies a substantial compaction (Figure S12B). However, there is another option that eJTM directly interacts with NGF and Pro residues facilitate this interaction.

Correct positioning of eJTM residues switches the conformation of the TrkA transmembrane domains

In our recent work, we demonstrated that cysteine cross-linking of eJTM at certain positions (K410, K411, blue in Figure 1A) results in the ligand-independent activation of TrkA (Franco et al., 2020). Here we undertook a structural investigation of the K410C mutant to find the mechanics of TrkA activation via the eJTM domain. As previously, we synthesized the isotope-labeled TrkA-eJTM-TMD-K410C and inserted it into the DMPC/CHAPS bicelles. Although the spectrum of the mutant was initially similar to the one of the TrkA-eJTM-TMD, eventually the transmembrane domain signals disappeared completely from the spectrum, most likely due to the high-order oligomerization induced by the C410 cross-linking. For this reason, we switched to the DPC micelles (Figure 5C), the environment that was used previously to elucidate the structure of dimeric TrkA TMDs (Franco et al., 2020). First, we found that the wild-type TrkA-eJTM-TMD
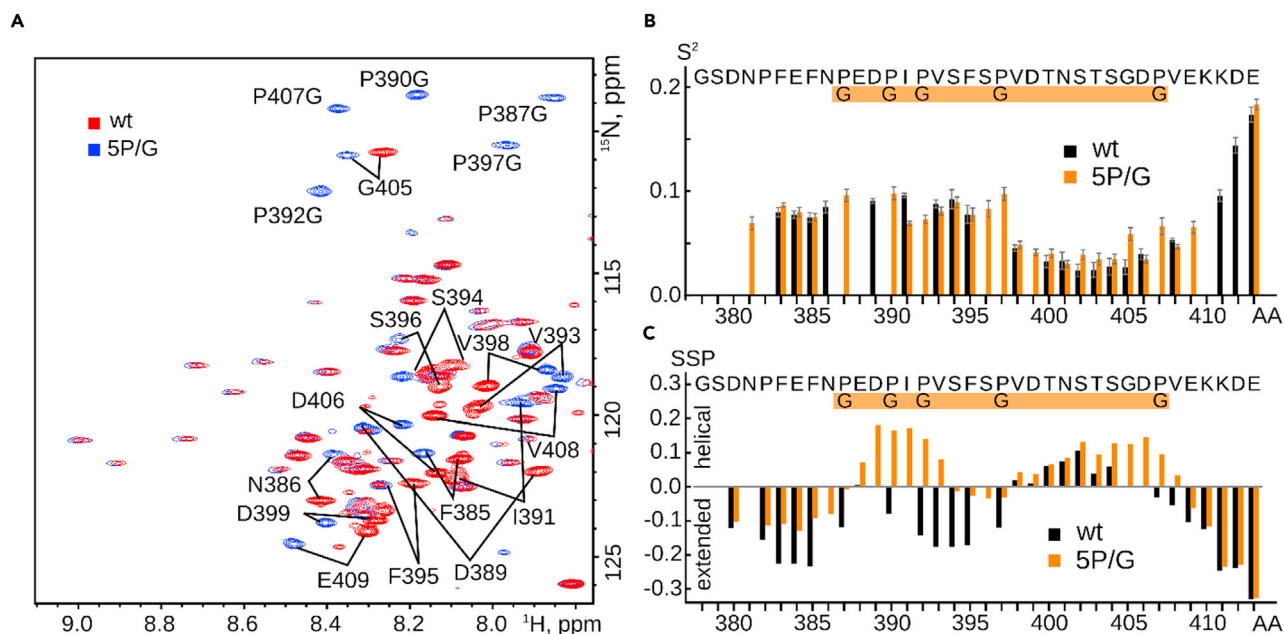
Figure 4. Conformation of TrkA-eJTM-5P/G

(A) An overlay of ^{1}H-^{15}N-TROSY-HSQC spectra of wt (in red) and 5P/G mutant (in blue) of TrkA-eJTM-TMD. The signals of mutant prolines and adjacent residues are indicated.

(B) S^{2} order parameter measured for the JM region of WT (in black) and 5P/G mutant (in orange).

(C) Secondary structure propensity calculated for the JM region of wt (in black) and 5P/G mutant (in orange) from NMR chemical shifts.

dimerization occurs via exactly the same interface as the short TMD, studied previously (Figure 5A) (Franco et al., 2020). The splittings of signals, observed in the NMR spectra of amide groups at low lipid-to-protein ratio are identical (Figures 5A and S13). The cross-peak positions, observed for the TMD of the TrkA-eJTM-TMD-K410C monomer, coincide with the positions found for the monomer of the wild-type protein (Figure 5B). However, when the disulfide cross-linking took place (Figure S12), we observed the presence of the new TMD state, with chemical shifts being drastically different from the wild-type TMD dimer (Figures 5B, S15, and S16). We characterized the rotational diffusion of the protein/micelle complex to elucidate the oligomeric state of the new TrkA eJTM form (Kot et al., 2020). According to our data, the hydrodynamic radius (Rh) of TrkA-eJTM-TMD dimer in DPC micelles equals 3.1 nm, and the same number was found for the cross-linked state or TrkA-eJTM-TMD-K410C (Figures 5D and S17). Taking into account that K410C mutation results in the spontaneous activation of TrkA, and that the previously resolved NMR structure of TrkA TMD in DPC micelles was shown to be physiologically relevant, according to mutagenesis (Franco et al., 2020), we can conclude that the cross-linking of eJTM at the position of K410 switches the conformation of the TMD dimer from the inactive state, which corresponds to the PDB ID 2N90, to the previously not structurally characterized active state (Franco et al., 2020).

DISCUSSION

To summarize, we show here that eJTM of TrkA is a flexible and intrinsically disordered region (IDR) that does not interact with the lipid membrane and bivalent cations. On the other hand, this region appears to be important for the functioning of the full-length protein; its deletion impairs the ligand binding and receptor activation, and substitution of conservative proline residues in eJTM can inhibit TrkA activation by NGF. At the same time, these proline mutations do not affect the mobility of the region and only slightly influence its average structure and compactness. Moreover, the eJTM region does not get structured upon the dimerization of the receptor TMD. Finally, we show that cross-linking of eJTM can alter the structure of TMD dimer, switching it from the inactive to the active state (Franco et al., 2020). Thus, we have to state that flexible and disordered juxtamembrane regions need to somehow couple the states of the extracellular and transmembrane domains of TrkA to transfer the information on the ligand binding inside the cell, and this looks hardly possible.
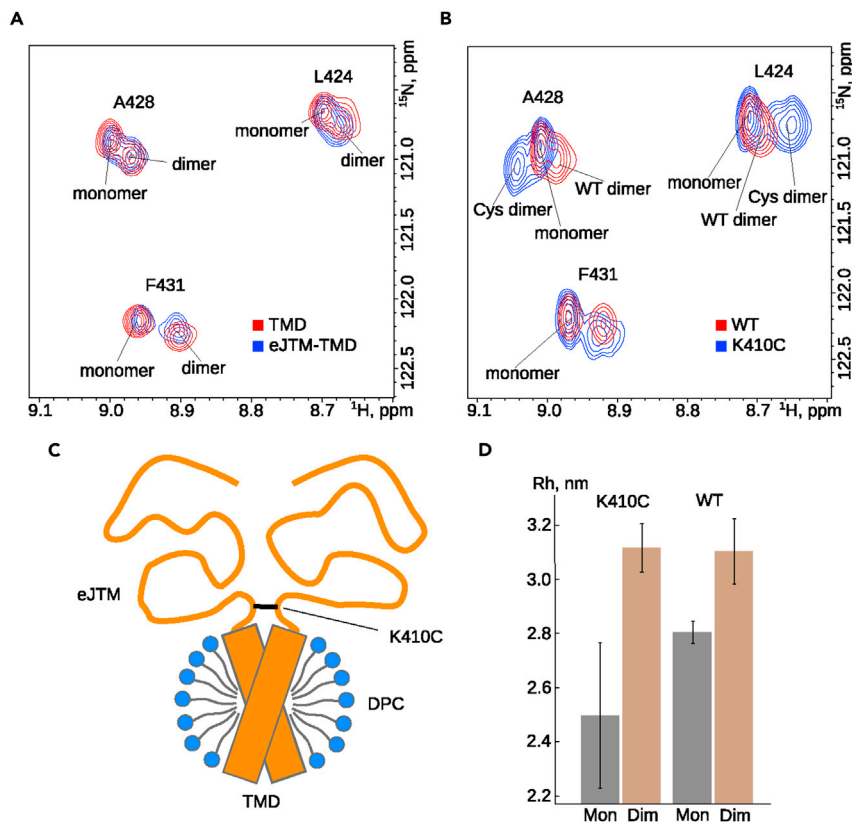
Figure 5. Crosslinking of eJTM-K410C induces the active conformation of the TMD

(A) An overlay of ^1H-^{15}N-HSQC spectra of TrkA-eJTM-TMD (blue) and TrkA-TMD, which lacks the eJTM region (red) in DPC micelles at pH = 5.9, 318K. Spectrum of TrkA-TMD was acquired for our previous study (Franco et al. 2020). Assignment of cross-peaks to the TrkA-eJTM-TMD residues is indicated.

(B) An overlay of ^1H-^{15}N-HSQC spectra of WT (red) and C410-crosslinked covalent dimer of K410C mutant (blue) of TrkA-eJTM-TMD in DPC micelles at pH = 5.9, 318K.

(C) Schematic drawing showing the covalent dimer of TrkA-eJTM-TMD-K410C in DPC micelle.

(D) Hydrodynamic radii of WT and K410C monomeric and dimeric forms, obtained from the cross-correlated relaxation rates of the protein amide groups.

With this in mind we would like to put forward a hypothesis that flexible eJTM regions of TrkA govern the conformation of the TMD by the direct interaction with the ligand. The stated hypothesis can find supporting evidence both in our experiments and in the literature. First, our recent work (Franco et al., 2020) reports the results of Cys-scanning mutagenesis in the C-terminal part of eJTM. These data reveal that cross-linking of eJTM at a very certain region of K410-K411 is necessary to trigger the ligand-independent activation of TrkA (Franco et al., 2020). This site is adjacent to the TMD, which starts at V418 and is far away from the ligand-binding TrkA-d5 domain, which ends at D380 (Figure 6). This implies that the ligand binding to the TrkA-d5-domain should cause the proximity of the region that is 30 flexible residues apart, which is impossible, if we assume the absence of interactions between the eJTM and NGF.

Next, we showed that mutations of proline residues to glycines inhibit the NGF binding to TrkA and NGF-induced activation of the receptor. On the other hand, NMR experiment demonstrated that prolines do not restrict the mobility of eJTM and the 5P/G mutation imposes a slight effect on the structure and compactness of the region. This implies that prolines are needed not to make the eJTM more rigid, but for some other reason, and direct interaction with NGF in the proper orientation is the best possible option. Although prolines are usually referred to as "disorder-promoting" residues (Theillet et al., 2013), they are also known to be highly important for the protein-protein interactions that involve the IDRs. In particular, proline-rich regions were found to adopt a unique PPII-helix structure, which represents a common protein-binding interface, recognized by specific domains, e.g., SH3 and WW domains
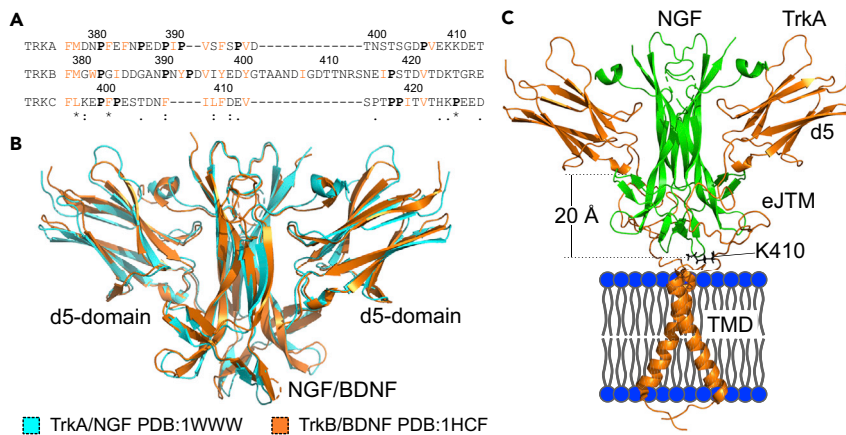
Figure 6. Conservation of the eJTM region in Trk recepotrs

(A) Alignment of eJTM regions of three human Trk receptors. Proline residues are in bold; hydrophobic and aromatic residues are shown in orange.

(B) Superposition of crystal structures solved for the complex of TrkA-d5 domain with NGF (cyan, PDB: 1WWW) and the complex of TrkB-d5 domain with BDNF (orange, PDB: 1HCF).

(C) Schematic representation of the NGF/TrkA complex based on the crystal structure of the NGF/TrkA-d5 complex (PDB: 1WWW) and the NMR structure of TrkA-TMD dimer in DPC micelles (PDB: 2N90). d5, TrkA-d5 domain of TrkA; eJTM, extracellular juxtamembrane region of TrkA; TMD, transmembrane domain of TrkA. The location of Lys410 is indicated.

([Rath et al., 2005](#)). Multiple proteins that recognize IDRs require prolines at certain positions, including the well-known enzymes (trombin, sortase A) and intracellular adapter proteins (TRAFs) ([Park, 2018](#)).

Last, one can analyze the ligand specificity and spatial structures of the three human Trks. Superposition of NGF and BDNF structures in complex with TrkA and TrkB (PDB 1WWW and 1HCF [[Banfield et al., 2001](#); [Wiesmann et al., 1999](#)]) reveals that they are almost completely identical ([Figure 6](#)), including the distance between the C terminus of TrkA-d5 domain and the "bottom" of the ligand. In contrast, primary protein sequences of their eJTM regions differ drastically: eJTM of TrkB is 15 residues longer and contains only three prolines, compared with six in TrkA. Fifteen-residues insert is much greater than the observed ~0.2 nm compaction of eJTM upon the 5P/G substitution, suggesting that the length of eJTM is not a major factor, governing the receptor activation. Therefore, similar to TrkA/NGF extracellular TrkB/BDNF complex needs to be coupled to the state of the TMD via the extremely long flexible linker, which, unlike TrkA, contains no possible elements that could restrict its mobility. In this regard, the direct eJTM/ligand interaction is one of the most probable options that could explain the activation of such distinct proteins by the same initial stimuli. Certainly, one cannot exclude the possibility that eJTM region is also interacting with the TrkA-d5 domain, which could make it structured and more regular. However, the fact that eJTM regions may alter the ligand specificity of Trk receptors still supports the hypothesis of direct eJTM/NGF interaction. The two splicing variants of TrkA that either contain the six-residue fragment VSFSPV in the proline-rich region of eJTM or lack it were shown to have similar binding affinity to NGF, whereas only the longer protein is capable of NT-3-induced activation ([Clary and Reichardt, 1994](#)). Similarly, TrkB transcripts lacking the 11-residue exon in eJTM reveal the altered specificity to NT-3 and NT4/5, whereas the specificity to BDNF is preserved ([Strohmaier et al., 1996](#)). The overall shape and length of neurotrophins NT-3 and NT4/5 does not differ from NGF and BDNF.

To conclude, we show here that eJTM regions of TrkA are intrinsically disordered, but are important for receptor activation. Joint analysis of obtained structural and functional data suggests that eJTMs are likely to interact directly with the ligand. This interaction could result in the proximal positions of the membrane-adjacent residues of eJTM, which, in turn, would switch the conformation of transmembrane helices.

Limitations of the study

One of the main limitations of the study is the use of a truncated protein lacking the TrkA-d5 domain, which precludes the direct high-resolution investigation of the NGF interaction with the eJTM region.

STAR★METHODS

Detailed methods are provided in the online version of this paper and include the following:

- KEY RESOURCES TABLE
- RESOURCE AVAILABILITY
  - Lead contact
  - Materials availability
  - Data and code availability
- METHODS DETAILS
  - DNA constructs
  - Cell culture and transfection
  - Western blot analysis
  - Differentiation of PC12nnr5 cells
  - Immunofluorescence and confocal microscopy
  - Cell surface expression by flow cytometry
  - TrkA/NGF-biotin binding assay by flow cytometry
  - Cell-free synthesis of TrkA-eJTM-TMD for NMR studies
  - Sample preparation for NMR studies
  - NMR spectroscopy and data processing
- QUANTIFICATION AND STATISTICAL DETAILS

SUPPLEMENTAL INFORMATION

Supplemental information can be found online at https://doi.org/10.1016/j.isci.2022.104348.

AUTHOR CONTRIBUTIONS

E.F.K performed the NMR experiments and analyzed the data, E.V.V and A.V.S synthesized the proteins for NMR studies, and M.L.F. constructed the TrkA mutants and performed the TrkA activation, differentiation, functional, binding, and crosslinking experiments. S.A.G., K.S.M, A.S.A., and M.V. designed and supervised the entire project and wrote the manuscript.

DECLARATION OF INTERESTS

The authors declare no competing interests.

REFERENCES

Arevalo, J.C., Conde, B., Hempstead, B.I., Chao, M.V., Martín-Zanca, D., and Pérez, P. (2001). A novel mutation within the extracellular domain of TrkA causes constitutive receptor activation. Oncogene 20, 1229–1234. https://doi.org/10.1038/sj.onc.1204215.

Banfield, M.J., Naylor, R.L., Robertson, A.G., Allen, S.J., Dawbarn, D., and Brady, R.L. (2001). Specificity in Trk receptor:neurotrophin interactions: the crystal structure of TrkB-d5 in complex with neurotrophin-4/5. Structure 9, 1191–1199. https://doi.org/10.1016/s0969-2126(01)00681-5.

Cavanagh, J. (2006). Protein NMR Spectroscopy: Principles and Practice (Academic Press).

Chill, J.H., Louis, J.M., Baber, J.L., and Bax, A. (2006). Measurement of 15N relaxation in the detergent-solubilized tetrameric KcsA potassium channel. J. Biomol. NMR 36, 123–136. https://doi.org/10.1007/s10858-006-9071-4.

Clary, D.O., and Reichardt, L.F. (1994). An alternatively spliced form of the nerve growth factor receptor TrkA confers an enhanced response to neurotrophin 3. Proc. Natl. Acad. Sci.

U S A 91, 11133–11137. https://doi.org/10.1073/pnas.91.23.11133.

Dosset, P., Hus, J.C., Blackledge, M., and Marion, D. (2000). Efficient analysis of macromolecular rotational diffusion from heteronuclear relaxation data. J. Biomol. NMR 16, 23–28. https://doi.org/10.1023/a:1008305808620.

Endres, N.F., Barros, T., Cantor, A.J., and Kuriyan, J. (2014). Emerging concepts in the regulation of the EGF receptor and other receptor tyrosine kinases. Trends Biochem. Sci. 39, 437–446. https://doi.org/10.1016/j.tibs.2014.08.001.

Erdős, G., and Dosztányi, Z. (2020). Analyzing protein disorder with IUPred2A. Curr. Protoc. Bioinformatics *70*, e99. https://doi.org/10.1002/cpbi.99.

Farrow, N.A., Muhandiram, R., Singer, A.U., Pascal, S.M., Kay, C.M., Gish, G., Shoelson, S.E., Pawson, T., Forman-Kay, J.D., and Kay, L.E. (1994). Backbone dynamics of a free and a phosphopeptide-complexed src homology 2 domain studied by 15N NMR relaxation. Biochemistry *33*, 5984–6003. https://doi.org/10.1021/bi00185a040.

Favier, A., and Brutscher, B. (2011). Recovering lost magnetization: polarization enhancement in biomolecular NMR. J. Biomol. NMR *49*, 9–15. https://doi.org/10.1007/s10858-010-9461-5.

Fischer, H., Polikarpov, I., and Craievich, A.F. (2004). Average protein density is a molecular-weight-dependent function. Protein Sci. *13*, 2825–2828. https://doi.org/10.1110/ps.04688204.

Franco, M.L., Nadezhdin, K.D., Goncharuk, S.A., Mineev, K.S., Arseniev, A.S., and Vilar, M. (2020). Structural basis of the transmembrane domain dimerization and rotation in the activation mechanism of the TRKA receptor by nerve growth factor. J. Biol. Chem. *295*, 275–286. https://doi.org/10.1074/jbc.ra119.011312.

Franco, M.L., Nadezhdin, K.D., Light, T.P., Goncharuk, S.A., Soler-Lopez, A., Ahmed, F., Mineev, K.S., Hristova, K., Arseniev, A.S., and Vilar, M. (2021). Interaction between the transmembrane domains of neurotrophin receptors p75 and TrkA mediates their reciprocal activation. J. Biol. Chem. *297*, 100926. https://doi.org/10.1016/j.jbc.2021.100926.

Gast, K., and Fiedler, C. (2012). Dynamic and static light scattering of intrinsically disordered proteins. Methods Mol. Biol. *896*, 137–161. https://doi.org/10.1007/978-1-4614-3704-8_9.

Green, S.H., Rydel, R.E., Connolly, J.L., and Greene, L.A. (1986). PC12 cell mutants that possess low- but not high-affinity nerve growth factor receptors neither respond to nor internalize nerve growth factor. J. Cell Biol. *102*, 830–843.

Kot, E.F., Goncharuk, S.A., Arseniev, A.S., and Mineev, K.S. (2018). Phase transitions in small isotropic bicelles. Langmuir *34*, 3426–3437. https://doi.org/10.1021/acs.langmuir.7b03610.

Kot, E.F., Wang, Y., Goncharuk, S.A., Zhang, B., Arseniev, A.S., Wang, X., and Mineev, K.S. (2020). Oligomerization analysis as a tool to elucidate the mechanism of EBV latent membrane protein 1 inhibition by pentamidine. Biochim. Biophys. Acta Biomembr. *1862*, 183380. https://doi.org/10.1016/j.bbamem.2020.183380.

Lemmon, M.A., and Schlessinger, J. (2010). Cell signaling by receptor tyrosine kinases. Cell *141*, 1117–1134. https://doi.org/10.1016/j.cell.2010.06.011.

Marsh, J.A., Singh, V.K., Jia, Z., and Forman-Kay, J.D. (2006). Sensitivity of secondary structure propensities to sequence differences between alpha- and gamma-synuclein: implications for fibrillation. Protein Sci. *15*, 2795–2804. https://doi.org/10.1110/ps.062465306.

Mészáros, B., Erdos, G., and Dosztányi, Z. (2018). IUPred2A: context-dependent prediction of protein disorder as a function of redox state and protein binding. Nucleic Acids Res. *46*, W329–W337. https://doi.org/10.1093/nar/gky384.

Mineev, K.S., Nadezhdin, K.D., Goncharuk, S.A., and Arseniev, A.S. (2016). Characterization of small isotropic bicelles with various compositions. Langmuir *32*, 6624–6637. https://doi.org/10.1021/acs.langmuir.6b00867.

Park, H.H. (2018). Structure of TRAF family: current understanding of receptor recognition. Front. Immunol. *9*, 1999. https://doi.org/10.3389/fimmu.2018.01999.

Rath, A., Davidson, A.R., and Deber, C.M. (2005). The structure of "unstructured" regions in peptides and proteins: role of the polyproline II helix in protein folding and recognition. Biopolymers *80*, 179–185. https://doi.org/10.1002/bip.20227.

Sklar, L.A., Edwards, B.S., Graves, S.W., Nolan, J.P., and Prossnitz, E.R. (2002). Flow cytometric analysis of ligand-receptor interactions and molecular assemblies. Annu. Rev. Biophys. Biomol. Struct. *31*, 97–119. https://doi.org/10.1146/annurev.biophys.31.082901.134406.

Strohmaier, C., Carter, B.D., Urfer, R., Barde, Y.A., and Dechant, G. (1996). A splice variant of the neurotrophin receptor trkB with increased specificity for brain-derived neurotrophic factor. EMBO J. *15*, 3332–3337. https://doi.org/10.1002/j.1460-2075.1996.tb00698.x.

Theillet, F.-X., Kalmar, L., Tompa, P., Han, K.-H., Selenko, P., Dunker, A.K., Daughdrill, G.W., and Uversky, V.N. (2013). The alphabet of intrinsic disorder. Proteins *1*, e24360. https://doi.org/10.4161/idp.24360.

Tyn, M.T., and Gusek, T.W. (1990). Prediction of diffusion coefficients of proteins. Biotechnol. Bioeng. *35*, 327–338. https://doi.org/10.1002/bit.260350402.

Ultsch, M.H., Wiesmann, C., Simmons, L.C., Henrich, J., Yang, M., Reilly, D., Bass, S.H., and de Vos, A.M. (1999). Crystal structures of the neurotrophin-binding domain of TrkA, TrkB and TrkC 1 1Edited by I. A. Wilson. J. Mol. Biol. *290*, 149–159. https://doi.org/10.1006/jmbi.1999.2816.

Urfer, R., Tsoulfas, P., O'Connell, L., Hongo, J.A., Zhao, W., and Presta, L.G. (1998). High resolution mapping of the binding site of TrkA for nerve growth factor and TrkC for neurotrophin-3 on the second immunoglobulin-like domain of the Trk receptors. J. Biol. Chem. *273*, 5829–5840. https://doi.org/10.1074/jbc.273.10.5829.

Wehrman, T., He, X., Raab, B., Dukipatti, A., Blau, H., and Garcia, K.C. (2007). Structural and mechanistic insights into nerve growth factor interactions with the TrkA and p75 receptors. Neuron *53*, 25–38. https://doi.org/10.1016/j.neuron.2006.09.034.

Wiesmann, C., Ultsch, M.H., Bass, S.H., and de Vos, A.M. (1999). Crystal structure of nerve growth factor in complex with the ligand-binding domain of the TrkA receptor. Nature *401*, 184–188. https://doi.org/10.1038/43705.

Wilken, H.C., Rogge, S., Götze, O., Werfel, T., and Zwirner, J. (1999). Specific detection by flow cytometry of histidine-tagged ligands bound to their receptors using a tag-specific monoclonal antibody. J. Immunol. Methods *226*, 139–145. https://doi.org/10.1016/s0022-1759(99)00064-2.

Zaccaro, M.C., Ivanisevic, L., Perez, P., Meakin, S.O., and Saragovi, H.U. (2001). p75 Co-receptors regulate ligand-dependent and ligand-independent Trk receptor activation, in part by altering Trk docking subdomains. J. Biol. Chem. *276*, 31023–31029. https://doi.org/10.1074/jbc.m104630200.

STAR★METHODS

KEY RESOURCES TABLE

REAGENT or RESOURCE	SOURCE	IDENTIFIER
Antibodies		
Rabbit Anti-TrkA, phospho (Tyr674/Tyr675) Monoclonal Antibody, Unconjugated, Clone C50F3	Cell Signaling Technology	Cat# 4621 RRID: AB_916186
Anti-TrkA antibody	Millipore	Cat# 06-574,RRID: AB_310180
IRDye 680LT Goat anti-Mouse IgG antibody	LI-COR Biosciences	Cat# 925-68020,RRID: AB_2687826
IRDye 800CW Goat anti-Rabbit IgG antibody	LI-COR Biosciences	Cat# 925-32211 RRID: AB_2651127
Anti-β-Actin Antibody	Sigma-Aldrich	Cat# A5441 RRID: AB_476744
Cy2 Conjugated Streptavidin antibody	Jackson ImmunoResearch Labs	Cat# 016-220-084 RRID: AB_2337246
Anti-NGF antibody	SIGMA	Cat # N6655; RRID: AB_477660
Bacterial and virus strains		
E. coli BL21(DE3) competent cells	Evrogen	CC002
Chemicals, peptides, and recombinant proteins		
CHAPS	Anatrace	C316S
DMPC	Anatrace	D514
DPC	Avanti Polar Lipids	850336P
The gene encoding wt TrkA-eJTM-TMD	UniProt	P04629
NGF	Alomone	N-100
Sodium creatine phosphate dibasic	Sigma-Aldrich	27920
Lithium potassium acetyl phosphate	Sigma-Aldrich	A0262
DL-Dithiothreitol	Sigma-Aldrich	D9779
Uridine 5′-triphosphate trisodium salt dihydrate	Sigma-Aldrich	94370
Uridine 5′-triphosphate trisodium salt dihydrate	Sigma-Aldrich	94370
Guanosine 5′-triphosphate sodium salt hydrate	Sigma-Aldrich	51120
Cytidine 5′-triphosphate disodium salt hydrate	Sigma-Aldrich	30320
Adenosine 5′-triphosphate trisodium salt dihydrate	Calbiochem	1191
Folinic acid calcium salt hydrate	Sigma-Aldrich	47612
PEG 8000	Sigma-Aldrich	41009
COmplete	Roche	05056489001
Sodium azide	Sigma-Aldrich	S2002
Creatine kinase	Roche	10127566001
tRNA	Roche	10109541001
RiboLock RNase Inhibitor	ThermoFisher	EO0381
Tris	Merck	K39103087
NaCl	Реахим	130314
N-Lauryl sarcosine sodium salt	Merck	S5120415
Imidazole	Sigma-Aldrich	792527
2-Mercaptoethanol	helicon	Am-O482
Sodium orthovanadate	Sigma-Aldrich	S6508
Sodium fluoride	Sigma-Aldrich	215309

Continued

REAGENT or RESOURCE	SOURCE	IDENTIFIER
Critical commercial assays		
Bradford kit (Pierce)	Thermofisher	#23236
Quick Change Site-directed mutagenesis kit	Aglient	#200519
Biotynilation kit sulfo-NHS-LC EZ-Link	Thermofisher	#21435
Deposited data		
wt TrkA-eJTM-TMD chemical shifts	BMRB	51343
5P/G TrkA-eJTM-TMD chemical shifts	BMRB	51344
K410C TrkA-eJTM-TMD chemical shifts	BMRB	51345
Raw data	Mendeley Data	https://data.mendeley.com/datasets/9rttm8wfr9/draft?a=e9777630-d584-4906-8adc-75bb570e2a89
NMR pulse code data	Mendeley Data	https://data.mendeley.com/datasets/9rttm8wfr9/draft?a=e9777630-d584-4906-8adc-75bb570e2a89
Experimental models: Cell lines		
HeLa cells	Human female	ATCC CRM-CCL-2
HEK-293 cells	Human female	ATCC CRL-1573
PC12 cells	Rat male	ATCC CRL-1721
PC12nnr5 cells	Rat male	Green et al., 1986
Oligonucleotides		
atggacaacccgttcgaattcaacccggaagacccgatcccggtttctt	Evrogen	taejmtm-f1
gtcaccagaggtagagttggtgtcaaccggagagaaagaaaccgggatcg	Evrogen	taejmtm-r1
atggacaacccgttcgaattcaacggtgaagacggcatcggtgtttctt	Evrogen	taejmtmp5g-f1
gtcaccagaggtagagttggtgtcaacgccagagaaagaaacaccgatgc	Evrogen	taejmtmp5g-r1
tctacctctggtgacccggttgaaaaaaaagatgaaaccccg	Evrogen	taejmtm-f2
atataaagcttggatccttatttgttgcggcggcc	Evrogen	tmtrkar
ttcatcttttttttcaacaccgtcaccagaggtaga	Evrogen	taejmtmp5g-r2
cggggtttcatctttgcattcaaccgggtcac	Evrogen	taejmtmk410-r1
tataggatccgacaacccgttc	Evrogen	taejtm-bam-f1
ataaagcttatcatttgttgcggcggc	Evrogen	tmtrka-rev
tataggatccgacaacccgttc	Evrogen	taejtm-bam-f1
ccttttgagttcaacggtgaggacggcatcggtgtctccttctcgcca	Integrated DNA technologies	TrkA eJTM 3P/G fw
tggcgagaaggagacaccgatgccgtcctcaccgttgaactcaaaagg	Integrated DNA technologies	TrkA eJTM 3P/G rev
gtctccttctcgggcgtggacactaac	Integrated DNA technologies	TrkA eJTM P397G fw
Gttagtgtccacgcccgagaaggagac	Integrated DNA technologies	TrkA eJTM P397G rev
Acatcaagagacggcgtggagaagaag	Integrated DNA technologies	TrkA eJTM P407G fw
Cttcttctccacgccgtctcttgatgt	Integrated DNA technologies	TrkA eJTM P407G rev
Cgcgtgaattcaaaagggttgtccataaag	Integrated DNA technologies	TrkA Del-eJTM fw
Cacgtgaattcacaccttttggggtctct	Integrated DNA technologies	TrkA Del-eJTM rev
Recombinant DNA		
A plasmid encoding rat TrkA with an N-terminal HA tag	pCDNA3.1	Dr. Yves Barde
Software and algorithms		
Bruker Topspin pulse program for Pseudo-3D DSTE-HSQC sequence	This paper; supplementary materials	dste_hsqc_13C_pr.zf.il_ek.txt
Wolfram Mathematica 5.0	Wolfram Research	-

Continued

REAGENT or RESOURCE	SOURCE	IDENTIFIER
Bruker Topspin	Bruker	3.2
CARA	R. Keller et al.	1.9.1.7
SSP	Joseph A. Marsh et al.	
GraphPad Prism 6	GraphPad Software	6.0e
Tensor	P. Dosset et al.	2
FACSDiva8 Software	BD Biosciences	-

RESOURCE AVAILABILITY

Lead contact

Further information and requests for resources and reagents should be directed to and will be fulfilled by the lead contact Marçal Vilar (mvilar@ibv.csic.es).

Materials availability

All the unique reagents (protein constructs and deletion mutants) developed in this work are available upon request.

Data and code availability

- Raw data is publicly available at Mendeley Data as of the date of publication. DOIs are listed in the Key resources table.

- The chemical shifts of the NMR experiments are deposited in the Biological Magnetic Resonance Data Bank (BMRB). Accession numbers are listed in the Key resources table.

- The NMR code developed here has been deposited in the Mendeley data and is publicly available as of the date of publication. DOIs are listed in the Key resources table.

METHODS DETAILS

DNA constructs

A plasmid encoding rat TrkA with an N-terminal HA tag was kindly provided by Dr. Yves Barde. TrkA is cloned in PCDNA3.1 with a N-terminal HA tag after the signal peptide sequence. All TrkA mutants and constructs were derived from this plasmid. Mutagenesis was done using the Quick Change Site-directed mutagenesis kit (Agilent) according to the manufacturer's protocol. The oligonucleotide sequences of all of the constructs are available upon request. All DNA constructs were sequenced using local facilities.

Cell culture and transfection

Hela cells, which do not express endogenous TrkA, were cultured in DMEM medium (Fisher) supplemented with 10% FBS (Fisher) at 37°C in a humidified atmosphere with 5% CO2. PC12 and PC12nnr5 cells were cultured in DMEM with 10% FBS and 5% horse serum (Fisher). Transfection of Hela cells was performed using polyethylenimine (PEI; Sigma) at a concentration of 1–2 mg/mL. The use of PEI as the transfection reagent for Hela cells resulted in suboptimal transfection (10–15% of cells transfected) and in the expression of only a small amount of TrkA in the cells. A concentration of 500–1000 ng of DNA per 10 cm cell plate was used for the TrkA activation experiments. Twenty-four hours after transfection the cells were lifted and re-plated into 12-well plates at a density of 100,000 cells per well. By using this procedure, the percentage of cells transfected was identical in all the wells. Forty-eight hours after transfection the cells were starved in serum free medium for 2 h and were then stimulated with NGF (Alomone) at the indicated concentrations and time intervals. Cells were lysed with TNE buffer (Tris-HCl pH 7.5, 150 mM NaCl, 1 mM EDTA) supplemented with 1% triton X-100 (Sigma), protease inhibitors (Roche), 1 mM PMSF (Sigma), 1 mM sodium orthovanadate (Sigma), and 1 mM sodium fluoride (Sigma). In the experiments involving the TrkA cysteine mutants, 10 mM iodoacetamide (Sigma) was added to the lysis buffer. Lysates were kept on ice for 10 minutes and centrifuged at 12,000 g for 15 minutes in a tabletop centrifuge. The protein level of the lysates was quantified using a Bradford kit (Pierce) and lysates were analyzed by SDS-PAGE.

Western blot analysis

Cellular debris was removed by centrifugation at 12,000 g for 15 minutes and the protein level of cell lysates was quantified using the Bradford assay (Pierce). Proteins were resolved in SDS-PAGE gels and transferred to nitrocellulose membranes that were incubated overnight at 4°C with one of the following antibodies: mouse monoclonal anti-HA (1:2000, Sigma); rabbit anti-phosphoTyr674/5 (1:1000, Cell Signaling); rabbit anti-TrkA (1:1000, Millipore). Following incubation with the appropriate secondary antibody labeled with near-infrared fluorophores; IR-680 or IR-800. Membranes were imaged and bands quantified using enhanced Li-Cor Odyssey equipment.

Differentiation of PC12nnr5 cells

Transfection in PC12nnr5 cells was performed using Lipofectamine 2000 as per manufacturer instructions. The mutant or the wild-type TrkA-transfected cells and mock-transfected cells as well as non-transfected cells were treated under the same conditions in a six-well tissue culture plate. The cells were washed three times with serum-free medium and incubated for 48 h in a medium containing 1% fetal bovine serum and 50 ng/mL of NGF (Alomone). At time 0, 24 h and 48 h, cells were washed with cold PBS and fixed with 4% paraformaldehyde during 15 minutes at room temperature. Cells were imaged using a Leica SP8 spectral confocal microscope. The percentage of cells with a neurite twice longer as the cell body was counted as differentiated.

Immunofluorescence and confocal microscopy

Transfected cells were fixed in coverslips with 4% paraformaldehyde in PBS for 10 min at room temperature. Coverslips were washed three times in PBS and were incubated with blocking buffer (0.1 M phosphate buffer and 3% FBS) at room temperature for 1 h to avoid non-specific binding. Cells were then incubated with the primary antibody (mouse anti-HA 12CA5 antibody (SIGMA) dilution 1:100) diluted in blocking buffer overnight at 4°C. Primary antibody was removed and coverslips were washed with 0.1 M PB three times and were incubated with the second antibody (anti-mouse Ig Alexa 555, number A31570 Invitrogen) diluted in 0.1 M phosphate buffer for 1 h at room temperature. Following washing with PBS three times for 5 min DAPI nuclear staining was added to the coverslips for 10 min and then washed. Coverslips were mounted with a drop of mounting medium. Cells were imaged in a Leica SP8 spectral confocal microscope using a 60× (oil) magnification. Proteins were imaged with fluorescence at the wavelengths of 561 nm (red) and 405 nm (DAPI – DNA staining).

Cell surface expression by flow cytometry

For detection of cell surface expression of TrkA mutants 10^6 cells were incubated in suspension with 200 μL of mouse anti-HA as described for immunocytochemistry for 30 min at 4°C to avoid receptor internalization. After incubation the cells were washed two times in ice-cold PBS by centrifugation for 5 min at 800 rpm and resuspended with 100 μL of the secondary antibody (anti-mouse Ig Alexa 488, number A21206 Invitrogen, dilution 1:100) for 30 min at 4°C in the dark. Two washes with ice-cold PBS were realized before analyze the cells with the flow cytometer. Cells were analyzed on a Miltenyi MACS10 cytometer.

TrkA/NGF-biotin binding assay by flow cytometry

Flow cytometry analysis of receptor/ligand interactions has been used in several systems (Sklar et al., 2002). We adapted a protocol described in (Wilken et al., 1999), using biotinylated NGF as a ligand. Briefly, TrkA-wt, ΔeJTM and P/G DNA constructs were transfected in Hela cells. NGF (Alomone) was biotinylated *in vitro* using EZ-Link Sulfo-NHS-Biotin reagent from Thermo Scientific following manufacturer protocol. Functional assessment of biotinylated NGF was performed by western blotting, and neurite differentiation in PC12 cells as shown in Figure S1. Total populations of transfected adherent cells were dissociated into a single cell suspension, washed with cold PBS containing 10 μM sodium azide and counted to use 5×10^5 cells per tube. The cells of each mutant were incubated with increasing concentration of NGF-Biotin (0, 1, 10, 100, 500 and 1000 ng/mL) for 15 min at 4°C. Cells were washed two times in ice-cold PBS by centrifugation for 5 min at 800 rpm and resuspended with 200 μL of diluted streptavidin Cy2 antibody (dilution 1:500) for 30 min at 4°C in dark. After being washed two times with ice-cold PBS Cells were analyzed on a Miltenyi MACS10 cytometer. Acquisition and analysis were performed with DiVa8 software using a 488-nm argon laser (green). Raw data is shown in Figure S1. Fluorescence intensity values versus increasing concentrations of NGF-biotin (in nM) were plotted and fitted to a one site total binding equation using GraphPad.

Cell-free synthesis of TrkA-eJTM-TMD for NMR studies

The gene encoding the juxtamembrane region and transmembrane domain of the human TrkA (380-447, UNIPROT P04629) was amplified by PCR using chemically synthesized oligonucleotides (Evrogen) and the gene of transmembrane domain which was described earlier (Table S1) (Franco et al., 2020) (Mineev et al., 2016). To assemble the TrkA-eJTM-TMD-5P/G (P387G/P390G/P392G/P397G/P407G) and TrkA-eJTM-TMD-K410C mutant, the oligonucleotides with corresponding mutations were used. The PCR products were cloned into a pGEMEX-1/H6tag vector by ligation using BamHI and HindIII restriction sites. The final constructs were confirmed by DNA sequencing (Table S2).

The proteins were produced using a cell-free continuous exchange expression system as described earlier (Franco et al., 2020). The cell-free reaction mixture was dialyzed against milli-Q water during 4 hours at room temperature. The lauroylsarcosine was added to the reaction mixture up to a final concentration of 0.5 %. The sample was incubated for 5 minutes, centrifuged at 25,000 g for 30 min and filtered using Millipore filter unit with 0.22 mkm pore size. The target protein was purified by immobilized metal affinity and size-exclusion chromatography. The soluble fraction was loaded to Ni Sepharose HP resin (Cytiva), which was pre-equilibrated with the IMAC-buffer (20 mM Tris, pH 8.0, 250 mM NaCl, 0.2% lauroylsarcosine) with 20 mM Imidazole. The target protein was washed by IMAC-buffer with 40 mM imidazole and eluted by IMAC-buffer with 500 mM Imidazole. The fractions with target protein were analyzed by SDS-PAGE, mixed and dialyzed at RT for 4 hours against 100x excess of SEC-buffer (10 mM Tris, pH 8.0, 50 mM NaCl, 0.2% lauroylsarcosine, 5 mM β-mercaptoethanol). The thrombin was added to the sample up to 5 U/mg and dialysis was continued overnight. The protein was concentrated up to 500 μL using Amicon filter device with 3 kDa pore size, filtered using Millipore filter unit and loaded to Tricorn 10/300 Superdex 200 increase column equilibrated in SEC-buffer. The fractions were analyzed by SDS-PAGE and the target protein was precipitated using TCA/Acetone procedure as described earlier (Franco et al., 2020).

Sample preparation for NMR studies

The powder of peptide was dissolved in 450 μL Trifluoroethanol (TFE) - water 2:1 mixture. Then we added the needed amounts of dimyristoyl phosphatidylcholine (DMPC) and 3-{Dimethyl[3-(3α,7α,12α-trihydroxy-5β-cholan-24-amido)propyl]azaniumyl}propane-1-sulfonate (CHAPS) or dodecylphosphocholine (DPC). Next, we evaporated the solvent on a lyophilic dryer and dissolved the sample in 450 μL of 20 mM NaPi buffer solution (pH = 6.4 in DMPC/CHAPS bicelles or 5.9 in DPC micelles) with 0.01% NaN$_3$ and 5% D$_2$O for frequency lock.

NMR spectroscopy and data processing

NMR spectra of TrkA samples in bicelles were acquired on Bruker Avance 800 MHz spectrometer (Bruker BioSpin, Germany) equipped with a cryogenic triple resonance probe at 40°C, to provide the optimal quality of NMR spectra of both TMD and eJTM residues. Spectra of the peptides in DPC micelles were acquired on Bruker Avance 600 MHz spectrometer with a cryogenic triple resonance probe at 45°C, to match the conditions of our previous study (Franco et al., 2020), which allows the direct comparison of NMR spectra. Pseudo-3D DSTE-HSQC diffusion spectra of TrkA-eJTM-TMD in bicelles were acquired on Bruker Avance 700 MHz with a room-temperature triple resonance probe at 40°C. Protein chemical shifts were assigned based on the set of triple-resonance spectra (HNCA, HN(CO)CA, HNCO, HN(CA)CO, HNCACB) , recorded employing the BEST approach (Favier and Brutscher, 2011) and ^{1}H,^{15}N-NOESY-HSQC in the CARA software. Standard procedure based on the interresidual correlations was utilized (Cavanagh, 2006). Chemical shifts of TrkA-eJTM-TMD and its mutants were deposited to the BMRB database under the accession codes BMRB ID 51343 (wt), 51344 (5P/G) and 51345 (K410C). Secondary structure propensities (SSP) were calculated from the NMR chemical shifts in the SSP software (Marsh et al., 2006).

Rotational correlation time and hydrodynamic radii of protein/lipid particles were derived from the cross-correlated relaxation ηxy of amide protons, as described (Chill et al., 2006; Kot et al., 2020). Longitudinal (R1) and transverse (R2) relaxation rates were measured using the corresponding Bruker Topspin sequences (hsqct1etf3gpsi.2 and hsqct2etf3gpsi, respectively) with minor modifications (Farrow et al., 1994). R1, R2, NOE and ηxy were calculated using Wolfram Mathematica 5.0. Generalized order parameters were calculated from the ^{15}N relaxation data using the model-free approach as implemented in Tensor 2 (Dosset et al., 2000).

To measure the hydrodynamic radii of a TrkA-eJTM-TMD-bicelle complex as a whole we designed a pulse sequence to acquire the pseudo-3D ^{1}H-^{13}C-HSQC diffusion spectra (Figure S7). For this, we added a DSTE 31 sequence fragment prior to an HSQC sequence (Bruker pulse sequence hsqcetgp). The result of this combined pulse sequence is an array of ^{1}H-^{13}C-HSQC spectra in which the intensities of signals are modulated with a known function of gradient strength (Figure S7). The diffusion delay (Δ) was set to 400 ms, pre-scan delay was 1s. Spectra were acquired in 24 scans with 32 dummy scans, 1024 points along the direct dimension (^{1}H) 66 points along the indirect dimension (^{13}C) and 16 points on the gradient dimension. Frequencies were centered on 4.7 ppm for 1H and 23 ppm for ^{13}C, spectral widths were 12 ppm for ^{1}H and 42 ppm for ^{13}C.

To interpret the obtained diffusion coefficient, we used the following approaches. (1) The measured diffusion coefficients were corrected taking into account the obstruction due to the high concentration and model of hard spheres to obtain the diffusion coefficients at infinite dilution $D0$. (2) D0 was converted to the hydrodynamic radii of an equivalent sphere (Rh) using the Stokes-Einstein equation:

$$D_0 = kT/6\pi\eta R_h,$$ (Equation 1)

Here k is the Boltzmann constant, T is the ambient temperature and η is the dynamic viscosity of solution. (3) To evaluate the "apparent" molecular weight of a complex corresponding to the measured $D0$ value we used the correlation obtained by Tyn and Gusek, 1990):

$$D = 5.78 \times 10^{-8} T/\eta R_g$$ (Equation 2)

This empirical equation determines the connection between the diffusion coefficient D and the gyration radius of protein, Rg. An equivalent globular protein can be described as a sphere having the radius Rg and the density of approximately 1.4 g/cm^3 (Fischer et al., 2004).

QUANTIFICATION AND STATISTICAL DETAILS

Tests used to determine statistical significance include the two-way ANOVA with Bonferroni correction (Figure 1E); the Dunnett's multiple comparison test (Figures 1F and 3C) and paired t test (Figure 3B). Statistical information for each experiment can be found in the figures and corresponding figure legend.